

## Thermal analysis of PDMS light bulbs with a luminophore

**Abstract.** This article focuses on the production and measurement of incandescent lamps made from polydimethylsiloxane and YAG luminophore. By a suitable combination of these materials along with a light source of a specific wavelength, white colour of light can be achieved. Since the optical power from the light source is fed through a light guide structure to a remote lighting section, the device can be used in hazardous environments such as mines or factories where electromagnetic interference is likely to occur. The study describes temperature characteristics and chromaticity temperature changes of the designed lamp for different luminophore concentrations.

**Streszczenie.** W artykule analizuje się lampy wykonane z polydimethylsiloxanu PDMS z luminoforem YAG. W lampach tych można osiągnąć białą barwę dzięki odpowiedniej kombinacji materiału. Dzięki odpowiedniej konstrukcji lampy te można używać w środowiskach niebezpiecznych jak kopalnie. W artykule analizowano temperaturę i barwę światła dla różnych luminoforów. **Analiza termiczna lamp PDM z luminoforem.**

**Keywords:** Polydimethylsiloxane (PDMS), luminophore, bulb, illumination, chromaticity temperature

**Słowa kluczowe:** PDM – polydimethylsiloxan, luminofor, barwa światła

### 1. Introduction

Polydimethylsiloxane (hereinafter referred to as PDMS) has been primarily designed to encapsulate photovoltaic cells, printed circuit boards, transformers, current sources, thermally stressed cables, optical connectors, etc. [1-3]. Later, it also began to be used for other purposes because it conveniently combines mechanical, electrical and optical properties.

In the 3D printing technology using the method of DPL (Digital Light Processing), it is used for the production of a printing base and is also widely used for fine lithography techniques, especially for the creation of microfluidic and microengineering systems - MEMS (Micro Electro Mechanical Systems). For example, the authors of the publication [4] describe an optical biopsy microsystem technology that has smaller dimensions (11.2 x 18.6 mm) compared to other systems and reduced power consumption. The microsystem includes an image magnification optical microsystem (IMOM) and light emitting diodes (LED). Microlenses made from PDMS are integrated into the IMOM subsystem to achieve image magnification and to improve LED illumination. Other interesting solutions in the field of MEMS systems are described by authors of publications [5-10]. Publication [11] describes a new construction of a hybrid multichannel optical sensor system designed to monitor patient's vital functions. The non-invasive measuring probe is based on two FBGs encapsulated in the polymer; the authors selected the PDMS polymer because it is inert. There was no deformation of the FBG sensors in the vulcanization process; after the vulcanization, a fourfold increase in temperature sensitivity was observed compared to the non-encapsulated FBG. The probe and the associated multichannel system offer the ability to monitor the basic vital functions (body temperature, heart rate and respiratory rate) in up to 128 patients. The same issue is addressed by the authors of publications [12-15].

Other application uses of PDMS include the segment of lighting and imaging technology, where new and innovative solutions are still sought. Thin 60 µm coatings made from PDMS are described by the authors of publication [16]. YAG luminescent particles, which exhibit a lack of red colour in the spectrum, are dispersed in the coatings and, therefore, red phosphorus based on nitride was dispersed in the coatings. Improvement in colour coating was caused by a suitable combination of two types of luminescent particles. Publication [17] describes multi-layered hybrid phosphorus structures for use in LEDs. The polycarbonate (PC) substrate is coated with a crosslinked PDMS layer

containing a yellow luminophore and, subsequently, a second layer with a red luminophore was applied. The separated layers emit white light in a shade of warm colour after excitation with a blue light source. The cold shade of white light can be achieved by dispersing yellow and red luminescent particles in one layer. Nevertheless, layered coatings exhibit improved optical properties compared to a coating prepared as a single layer. The authors of publication [18] confirm that thin crosslinked PDMS coatings containing luminescent particles of a yellow luminophore are very stable in terms of time. PDMS coatings were exposed to high temperatures (300 °C) and optical power (150 W) for a period of 21 days. Composite coatings were then examined by SEM and optical microscopy, and no cracking, discolouration, segregation, or significant degradation of the optical properties were observed.

Most lighting applications are based on a low-volume PDMS structure with luminophores, which is common with white LEDs [19-21]. In our work, we are testing large-volume PDMS structures with luminophores because we can combine them with powerful light sources.

### 2. Methods

So-called colorimetric systems are used for the objective characteristics of colours of the visible light. For precise colour characterization, it is necessary to know three items of data, so, in this case, we are talking about the trichromatic system. Their principle is based on the replacement of any colour stimulus with an additive mixture of three optimally selected specific colour stimuli. The individual colorimetric quantities of colour stimuli by means of which the additive mixture can produce the same colour perception as the intended coloured object are referred to as trichromatic components  $X, Y, Z$ . Colorimetric coefficients marked as  $\bar{x}(\lambda), \bar{y}(\lambda), \bar{z}(\lambda)$ , are used for their calculation. The trichromatic components (1-3) are then calculated by integrating the product of the relative spectral density of the radiant flux of colour stimulus and the colorimetric coefficient across the spectrum. [22]

$$(1) \quad X = \int_0^{\infty} \varphi_{e\lambda}(\lambda) \cdot \bar{x}(\lambda) d\lambda,$$

$$(2) \quad Y = \int_0^{\infty} \varphi_{e\lambda}(\lambda) \cdot \bar{y}(\lambda) d\lambda,$$

$$(3) \quad Z = \int_0^{\infty} \varphi_{e\lambda}(\lambda) \cdot \bar{z}(\lambda) d\lambda,$$

Colour tone, colour richness and colour intensity determine the resulting colour stimulus. These data are determined by three independent components of the trichromatic system, which can be illustrated in a three-

dimensional coordinate system (Figure 1a). The basic colours of all intensities are plotted on the axes in the resulting rectangular space. The lines passing through the beginning at point 0 express different colour tones. The brightness of the colour stimulus is not determined by the vector size  $\phi$ , but corresponds to the algebraic sum of the trichromatic components ( $X + Y + Z$ ). The  $\phi$  and  $\phi'$  colour stimuli lie on the same line because they have the same colour tone and richness. Their luminous fluxes are proportional and the following relation applies to them:  $\phi' = k \times \phi$ . On this basis, the colour stimulus can be described by a colorimetric equation. If we fit a plane onto the points marked on the axes, a coloured triangle is created in the colorimetric space (Figure 1b). [22]

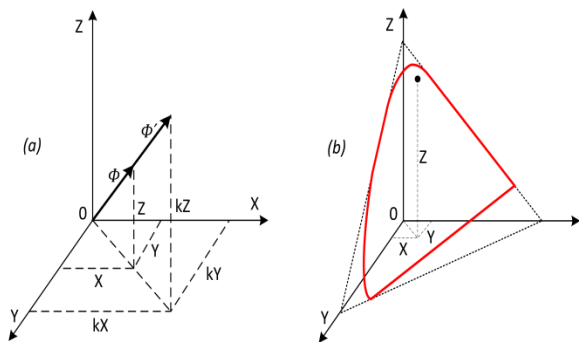


Fig. 1. (a) Spatial representation of a colour stimulus in the rectangular XYZ system, (b) a triangle in the plane  $X + Y + Z = 1$  of the rectangular colorimetric space.

Because the spatial representation is not very practical, a planar diagram is used to evaluate the colour stimulus in terms of tone and richness. The following applies to trichromatic coordinates

$$(4) \quad x = \frac{X}{X+Y+Z},$$

$$(5) \quad y = \frac{Y}{X+Y+Z},$$

$$(6) \quad z = \frac{Z}{X+Y+Z},$$

Thus, a CIE chromaticity diagram of the XYZ colorimetric system is created (Figure 3). At each vertex of the triangle, the basic colours (red, green, blue) of monochromatic light sources are located. The white colour of light can be obtained using an additive mixture of all the three basic colours.

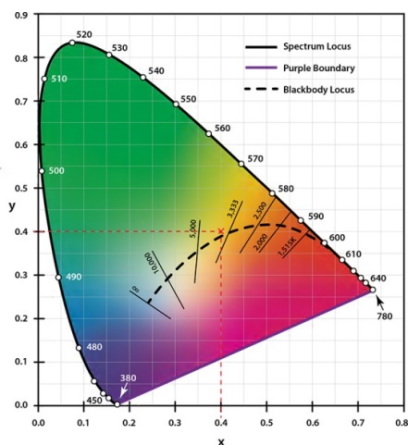


Fig. 2. A chromaticity diagram of the XYZ colorimetric system in the rectangular coordinates (x, y).

### 3. Experimental setup and measurement

The incandescent lamp was made from two-component silicone rubber called Sylgard 184 because it has ideal viscosity (5500 mPas) for our purposes. In a low viscosity solution, luminophore particles would clump at the bottom of the casting mould, since polymer vulcanization takes place for about 60 minutes at 100 °C. For high viscosity, it would probably not be possible to ensure a homogeneous distribution of luminophore particles, or this process would take too long. Using KERN PCB precision laboratory scales, the necessary amount of PDMS, into which the recommended curing agent was added, was weighed. Immediately after the addition of the curing agent, vulcanization begins, because this particular type of rubber can be cured even at room temperature. The prepared mixture was immersed in an ultrasonic bath for 15 minutes to degasify the mixture and to further homogenize the PDMS and the curing agent. Garnet luminophore  $Y_3Al_5O_{12}:Ce^{3+}$  in a defined weight ratio was fed into the mixture and the mixture thus prepared was placed into a rotary shaker to ensure a homogeneous distribution of the YAG luminophore in PDMS. The resulting homogeneous mixture was applied to a bulb-shaped glass mould in which we had implemented pre-prepared cylindrical light guide structures of the same material having a length of 25 mm and a diameter of 5 mm. The final shape of the incandescent lamp was placed in a temperature box to accelerate the vulcanization of the polymer (100 °C). At the last stage, the sample was subjected to 48-hour relaxation in a stable environment. The same procedure was repeated for other lamps. Figure 3 shows the final incandescent lamp made from PDMS with a yellow YAG luminophore.

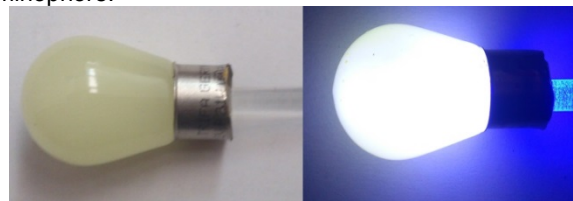


Fig. 3. An incandescent lamp made from PDMS.

The measuring station contains a 5 W laser source with a central wavelength of 455 nm, active cooling, an air aperture and a power supply. The measuring side consists of two temperature sensors (referred to as S\_1 and S\_2) and probes for chromaticity temperature measurement. The temperature sensors are of the K type; the manufacturer guarantees a resolution of 0.1 °C and an accuracy of 0.5 °C in the temperature range of -50 to +1300 °C. To read the temperature, the CEM DT-613 digital thermometer, which displays data from two measuring probes at the same time, was used. To assess the chromaticity temperature, a USB4000 spectrometer with a dynamic range of  $3.4 \times 10^6$  enabling measurement in the wavelength range from 200 to 1100 nm was used. Measurement of one lamp was conducted continuously for 12 hours, and every 20 minutes the temperature at defined points and the colour temperature of the output white light were recorded. Figure 4 shows the complete layout of the measuring station.

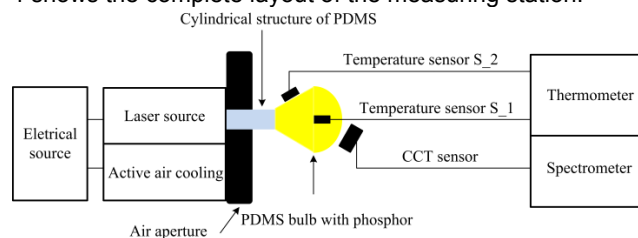


Fig. 4. The layout of the measuring station.

#### 4. Results

The weight relationship between the luminophore and PDMS was chosen based on past experience so that the resulting chromaticity temperature ranged in typical values for cooler tons of white light. Thirty incandescent lamps were produced from each weight ratio, i.e. the statistical data set includes the results measured on 210 samples. The graphs were produced based on average values.

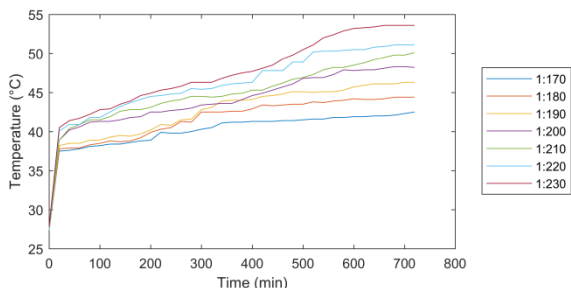


Fig. 5. Temperature characteristics of the lamp (S\_1).

Figure 5 shows the temperature characteristics measured by the S\_1 sensor located in the centre of the incandescent lamp. If an initial temperature (27.3 °C) that we recorded immediately after the activation of the light source is not included in the data set, the difference between the minimum and maximum values for the lowest weight ratio is 5 °C. At the highest weight ratio, the temperature increased by 13.1 °C. Table 1 compares temperature differences and dispersion of values for all weight ratios.

Table 1. Comparison of the values measured (S\_1).

Ratio	Temperature difference [°C]	Dispersion of values [-]
1:170	5.00	2.36
1:180	6.60	5.23
1:190	8.10	7.59
1:200	9.40	7.50
1:210	11.20	8.63
1:220	11.00	11.46
1:230	13.10	16.75

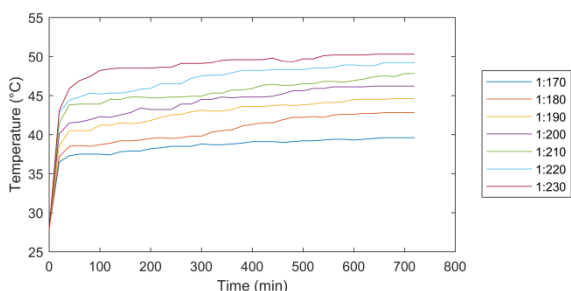


Fig. 6. Temperature characteristics of the lamp (S\_2).

Figure 6 shows the temperature characteristics measured by the S\_2 sensor located 2 mm under the surface of the lamp. The initial temperature of 27.7 °C is not again included in the statistical data set. At this measurement point, the temperatures do not reach the same values as in the previous case; in the middle of the lamp, heating is higher. The differences between the minimum and maximum temperatures are smaller by approximately a half with higher weight ratios. This is due to the good thermal conductivity of the polymer ( $0.146 \text{ W m}^{-1} \text{ K}^{-1}$ ); there is heat dissipation at the polymer/air interface. The biggest temperature difference is only 7.2 °C; all results are shown in Table 2.

The greatest chromaticity temperature variation was observed in a weight ratio of 1:230, namely 490 K. Lower weight ratios did not show such large variations (Table 3).

Table 2. Comparison of the temperatures measured (S\_2).

Ratio	Temperature difference [°C]	Dispersion of values [-]
1:170	3.10	0.63
1:180	5.60	2.65
1:190	6.00	2.18
1:200	6.10	2.74
1:210	6.30	1.89
1:220	6.40	2.67
1:230	7.20	2.01

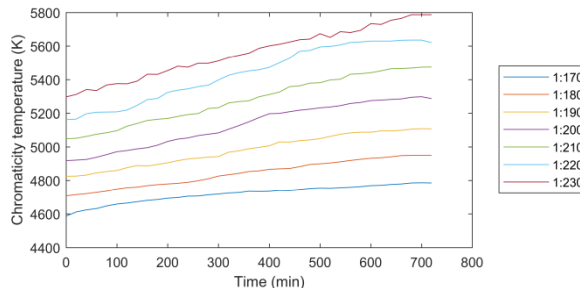


Fig. 7. Chromaticity temperature waveform.

Table 3. Chromaticity temperature variations for various weight ratios.

Ratio	Chromaticity temperature [K]
1:170	199
1:180	242
1:190	283
1:200	380
1:210	427
1:220	474
1:230	490

Figure 8 shows spectral behaviour of incandescent lamps with a weight ratio of 1:170. It can be seen that the intensity of radiation decreases with the increasing time or temperature. The biggest difference in the decrease is recorded after 90 minutes; later, the decreases are not so considerable. The same trend applies to other weight ratios; therefore, we state only one weight ratio. Only five spectra are shown in the graph because the other spectra overlap.

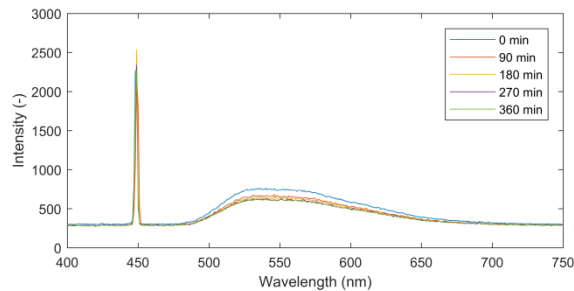


Fig. 8. Spectral dependence of a lamp with a weight ratio of 1:170.

#### 5. Conclusion

The functionality of the device has been verified for seven different weight ratios of the luminophore. The dimensions of the lamp correspond to a standard car bulb designed for turn indicators of a two-track vehicle with a length of 30 mm and a width of 25 mm in the widest part. The results show that the designed lamp is thermally stable in time. The highest temperature (53.6 °C) was recorded in the middle of the lamp by sensor S\_1; below the surface of the lamp, the highest temperature was slightly lower than 50.3 °C. Convective lamps generate a significantly higher temperature at the point of illumination, often above 130 °C, thus significantly reducing their service life. In our solution, we can separate the light source from the illuminating part, so the heat generated from the light source does not interfere with the illumination part. Especially in the automotive industry, it is considered a great advantage

because headlights generate a lot of heat in a small space. Chromaticity temperature of lamps changes only slightly over time; the human eye is not sensitive enough to notice this change.

### Acknowledgements

This article was supported by the Ministry of Education of the Czech Republic (Projects No. SP2018/170, SP2018/184, and SP2018/55). This research was partially supported by the Ministry of Education, Youth and Sports of the Czech Republic through Grant Project no. CZ.1.07/2.3.00/20.0217 within the framework of the Operation Programme Education for Competitiveness financed by the European Structural Funds and from the state budget of the Czech Republic. This article was also supported by the Ministry of the Interior of the Czech Republic within the projects Nos. VI20152020008 and VI2VS/444. This article was also supported by the Ministry of Industry and Trade of the Czech Republic within the project Nos. FV10396 and FV20581. This paper has been supported by the Grand Agency of the Czech Republic (project # 15-21547S). This work was supported by the European Regional Development Fund in the Research Centre of Advanced Mechatronic Systems project, project number CZ.02.1.01/0.0/0.0/16\_019/0000867 within the Operational Programme Research, Development and Education.

### Authors

Martin Novak, VSB - Technical university of Ostrava, Faculty of Electrical Engineering and Computer Science, Department of Telecommunications, 17. listopadu 15, 708 33 Ostrava-Poruba Czech Republic, E-mail: [martin.novak.st@vsb.cz](mailto:martin.novak.st@vsb.cz);  
Dr. Jan Nedoma, VSB - Technical university of Ostrava, Faculty of Electrical Engineering and Computer Science, Department of Telecommunications, 17. listopadu 15, 708 33 Ostrava-Poruba Czech Republic, E-mail: [jan.nedoma@vsb.cz](mailto:jan.nedoma@vsb.cz);  
Dr. Marcel Fajkus, VSB - Technical university of Ostrava, Faculty of Electrical Engineering and Computer Science, Department of Telecommunications, 17. listopadu 15, 708 33 Ostrava-Poruba Czech Republic, E-mail: [marcel.fajkus@vsb.cz](mailto:marcel.fajkus@vsb.cz);  
Assoc. Prof. Dr. Radek Martinek, VSB - Technical university of Ostrava, Faculty of Electrical Engineering and Computer Science, Department of Cybernetics and Biomedical Engineering, 17. listopadu 15, 708 33 Ostrava-Poruba Czech Republic, E-mail: [radek.martinek@vsb.cz](mailto:radek.martinek@vsb.cz).

### REFERENCES

- [1] B. Dudem, Y. H. Ko, J. W. Leem, J. H. Lim, and J. S. Yu, "Hybrid Energy Cell with Hierarchical Nano/Micro-Architected Polymer Film to Harvest Mechanical, Solar, and Wind Energies Individually/Simultaneously," ACS Applied Materials and Interfaces, vol. 8, pp. 30165-30175, 2016.
- [2] L. Yin, H. Z. Liu, Y. C. Ding, B. H. Lu, "Study on fabrication of 3D micro-structure in polymer photovoltaic cells based on nanoimprint lithography technology," Chinese Journal of Sensors and Actuators, vol. 19, pp. 1455-1458, 2006.
- [3] G. Chandra, J. Dodd, "Environmental and regulatory status of silicone transformer fluids," IEEE Conference Record of Annual Pulp and Paper Industry Technical Conference, pp. 148-152, 1995.
- [4] J. F. Ribeiro, A. C. Costa, et al., "PDMS Microlenses for Optical Biopsy Microsystems," IEEE Transactions on Industrial Electronics, vol. 64, pp. 9683-9690, 2017.
- [5] M. Rahbar, B. L. Gray, "Maximizing deflection in MEMS and microfluidic actuators fabricated in permanently magnetic composite polymers," 2017 IEEE 17th International Conference on Nanotechnology, art. no. 8117294, pp. 466-470, 2017.
- [6] J. Qu, W. Zhang, et. al., "Microscale Compression and Shear Testing of Soft Materials Using an MEMS Microgripper with Two-Axis Actuators and Force Sensors," IEEE Transactions on Automation Science and Engineering, vol. 14, art. no. 779523, pp. 834-843, 2017.
- [7] H. J. Pandya, J. Sheng, J. P. Desai, "MEMS-Based Flexible Force Sensor for Tri-Axial Catheter Contact Force Measurement," Journal of Microelectromechanical Systems, vol. 16, art. no. 7795258, pp. 264-272, 2017.
- [8] Y. Okayama, K. Nakahara, "Characterization of a bonding-in-liquid technique for liquid encapsulation into MEMS devices," Journal of Micromechanics and Microengineering, vol. 20, art. no. 095018, 2010.
- [9] A. Khosla, B. L. Gray, "Micropatternable multifunctional nanocomposite polymers for flexible soft NEMS and MEMS applications," ECS Transactions, vol. 45, pp. 477-494, 2012.
- [10] S. H. Yoon, V. Reyes-Ortiz, "Analysis of circular PDMS microballoons with ultralarge deflection for MEMS design," Journal of Microelectromechanical Systems, vol. 19, art. no. 5484661, pp. 854-864, 2010.
- [11] M. Fajkus, J. Nedoma, R. Martinek, V. Vasinek, H. Nazeran, P. Siska, "A non-invasive multichannel hybrid fiber-optic sensor system for vital sign monitoring," Sensors (Switzerland), vol. 17, art. no. 111, 2017.
- [12] J. Nedoma, M. Fajkus, P. Siska, R. Martinek, V. Vasinek, "Non-invasive fiber optic probe encapsulated into PolyDiMethylSiloxane for measuring respiratory and heart rate of the human body," Advances in Electrical and Electronic Engineering, vol. 15, pp. 93-100, 2017.
- [13] J. Nedoma, M. Fajkus, L. Bednarek, J. Frnda, J. Zavadil, V. Vasinek, "Encapsulation of FBG sensor into the PDMS and its effect on spectral and temperature characteristics," Advances in Electrical and Electronic Engineering, vol. 14, pp. 460-466, 2016.
- [14] J. Nedoma, M. Fajkus, V. Vasinek, "Influence of PDMS encapsulation on the sensitivity and frequency range of fiber-optic interferometer," Proceedings of SPIE - The International Society for Optical Engineering, vol. 9994, art. no. 99940P, 2016.
- [15] M. Fajkus, J. Nedoma, P. Siska, V. Vasinek, "FBG sensor of breathing encapsulated into polydimethylsiloxane," Proceedings of SPIE - The International Society for Optical Engineering, vol. 9994, art. no. 99940N, 2016.
- [16] J. Jia, H. S. Jia, et. al., "Highly Elastic and Flexible Phosphor Film for Flexible LED Lighting and Display Applications," Faguang Xuebao/Chinese Journal of Luminescence, vol. 38, pp. 1493-1502, 2017.
- [17] T. Güner, D. Köseoğlu, M. M. Demir, "Multilayer design of hybrid phosphor film for application in LEDs," Optical Materials, vol. 16, pp. 422-430, 2016.
- [18] A. C. C. Esteves, J. Brokken-Zijp, J. Laven, G. de With, "Light converter coatings from cross-linked PDMS/particles composite materials," Progress in Organic Coatings, vol. 68, pp. 12-18, 2010.
- [19] J. Vitasek, J. Jargus, J. S. Hejduk, T. Stratil, J. Latal, V. Vasinek, "Phosphor decay measurement and its influence on communication properties," International Conference on Transparent Optical Networks, art. no. 8024951, 2017.
- [20] L. C. Chen, W. W. Lin, J. W. Chen, "Fabrication of GaN-Based White Light-Emitting Diodes on Yttrium Aluminum Garnet-Polydimethylsiloxane Flexible Substrates," Advances in Materials Science and Engineering, vol. 2015, art. no. 537163, 2015.
- [21] T. Güner, U. Şentürk, M. M. Demir, "Optical enhancement of phosphor-converted wLEDs using glass beads," Optical Materials, vol. 72, pp. 769-774, 2017.
- [22] H. D. Zhao, H.-D. Y. Y. Yao, et. al., "Display the CIE 1931 color chromaticity diagram with digital image processing," Proceedings of SPIE - The International Society for Optical Engineering, vol. 9045, art. no. 904510, 2013.